nature physics

ARTICLES

PUBLISHED ONLINE: 8 DECEMBER 2014 | DOI: 10.1038/NPHYS3152

Strong magneto-chiral dichroism in a paramagnetic molecular helix observed by hard X-rays

Roberta Sessoli[1]*, Marie-Emmanuelle Boulon[1], Andrea Caneschi[1], Matteo Mannini[1], Lorenzo Poggini[1], Fabrice Wilhelm[2] and Andrei Rogalev[2]

Magneto-chiral dichroism is a non-reciprocal—that is, directional—effect observed in magnetized chiral systems, featuring an unbalanced absorption of unpolarized light depending on the direction of the magnetization. Despite the fundamental interest in a phenomenon breaking both parity and time-reversal symmetries, magneto-chiral dichroism is one of the least investigated aspects of light–matter interaction most likely because of the weakness of the effect in most reported experiments. Here we have exploited the element selectivity of hard X-ray radiation to investigate the magneto-chiral properties of enantiopure crystals of two isostructural molecular helicoidal chains comprising either cobalt(II) or manganese(II) ions. A strong magneto-chiral dichroism, with Kuhn asymmetry of the order of a few per cent, has been observed in the cobalt chains system, whereas it is practically absent for the manganese derivative. The spectral features of the X-ray magneto-chiral dichroism signal differ significantly from the natural and magnetic dichroic contributions and have been rationalized here using the multipolar expansion of matter–radiation interaction.

Interest in the interplay between chirality and magnetism dates back to Pasteur[1], but is still the subject of intense research[2], being relevant for a wide class of phenomena, ranging from exotic magnetic excitations known as skyrmions[3–5] to magneto-chiral conductance[6]. The interaction between light and matter is a powerful tool to investigate the simultaneous breaking of spatial symmetry—that is, the lack of inversion symmetry—and of time-reversal symmetry, as in the case of a magnetized non-centrosymmetric medium. Magnetism and chirality are indeed directly connected through the magneto-chiral dichroism (MχD) and birefringence[7–10], as was observed for the first time by Rikken and Raupach[11] in luminescence spectra and subsequently using X-ray radiation[12]. MχD is a non-reciprocal effect consisting in different absorption of unpolarized light by a chiral magnetized medium. It is a fascinating parity-violating phenomenon that has been suggested to be at the origin of homochirality of life on earth[13–15] as an alternative to electroweak nuclear interactions[16]. MχD is generally a very weak effect, with only a few examples reported[17–21] and a limited knowledge available of the factors that lead to the phenomenon.

The conditions of simultaneous breaking of parity and time-reversal symmetry required to observe the phenomenon are satisfied in magneto-electric media and multiferroics[22,23], but they can also be fulfilled in molecular paramagnetic and diamagnetic systems in the presence of an external magnetic field. The systems investigated here, consisting of isostructural molecular helicoidal chains comprising either anisotropic cobalt(II) or isotropic manganese(II) ions, can be considered intermediate between these two classes. A thorough investigation of the magneto-chiral effect through X-ray spectroscopy at the K-edge of the 3*d*-metals, evidencing a strong MχD in the cobalt chain system, is described.

We investigated two isostructural one-dimensional (1D) molecular chains of formula $[M(hfac)_2NITPhOMe]_\infty$, containing bi-positive metal ions ($M = Mn^{II}$ and Co^{II}) shielded by ancillary ligands ($hfac^- =$ hexafluoroacetylacetonato) and bridged by stable nitronyl-nitroxide organic radicals (NITPhOMe = 2-(4-methoxyphenyl)-4,4,5,5-tetramethylimidazoline-l-oxy1,3-oxide) carrying a delocalized unpaired electron[24,25]. The helical structure of $[M(hfac)_2NITPhOMe]_\infty$, shortened to $[M\text{-}NIT]_\infty$ hereafter, is generated in the crystalline phase by a three-fold screw axis (Fig. 1). Despite the absence of chiral constituents, the compounds form enantiopure crystals, crystallizing either in the chiral $P3_1$ or $P3_2$ space groups[24,25]. The crystals are optically active and exhibit a significant second-harmonic generation efficiency[26]. The magnetism of both compounds is governed by the strong intra-chain antiferromagnetic exchange interaction between the alternating paramagnetic metal ions and the spin $S = 1/2$ of the organic radicals, with exchange constant, $J = 235$ K and 495 K for the Co (ref. 27) and Mn (ref. 24) derivative, respectively. The exchange Hamiltonian for a chain of N spins is defined as $H_{ex} = J\sum_{i=1}^{N/2} s_{2i-1}S_{2i} + s_{2i+1}S_{2i}$, where the small s on odd sites represents the radical spin while the capital S on even sites represents either the Co^{II} or Mn^{II} spin. A completely different behaviour is, however, observed depending on the metal ion. In the case of Mn^{II}, Heisenberg 1D ferrimagnetic behaviour is observed owing to the lack of an orbital contribution for this d^5 ion, with strong long-range correlations and 3D ordering around $T = 5$ K induced by the weak inter-chain dipolar interactions[24]. In contrast, high-spin Co^{II} ions in an octahedral environment have a significant orbital moment, resulting in a strong magnetic anisotropy, with the easy axis of magnetization of each ion forming an angle of about 50° with the helix axis (Fig. 1a). Interestingly, the cobalt derivative was the first system exhibiting slowing down of the magnetization dynamics in the paramagnetic phase, as predicted by Glauber for

[1]Department of Chemistry 'Ugo Schiff' and INSTM Research Unit, University of Florence, 50019 Sesto Fiorentino, Italy. [2]European Synchrotron Radiation Facility (ESRF), 38043 Grenoble, France. *e-mail: roberta.sessoli@unifi.it

Table 1 | Different dichroic contributions to the radiation–matter interaction.

		Parity	Time reversal
XNCD	$E1M1+E1E2$	−	+
XMCD	$(E1E1+E2E2)M$	+	−
XMχD	$(E1M1+E1E2)M$	−	−

The involved mixed terms of the radiation–matter interaction and their parity behaviour are listed for each type of dichroism. *M* stands for the sample magnetization. For the sake of completeness we recall that other types of dichroism can be obtained with linearly polarized light. These are: X-ray natural linear dichroism (XNLD), X-ray magnetic linear dichroism (XMLD), which are both parity and time-reversal even, and non-reciprocal linear dichroism (NRLD), which is parity odd and time-reversal odd.

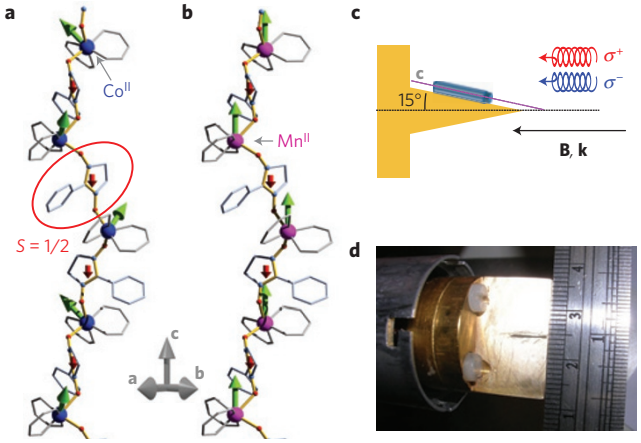

Figure 1 | Structures of the molecular magnetic helices and experimental set-up. a,**b**, View of the simplified structure of the [M-NIT]$_\infty$ molecular helices containing Co^{II} (**a**) and Mn^{II} (**b**) ions bridged by organic nitronyl-nitroxide radicals, with a radical unit highlighted by the red circle. The metal ions are highlighted as large spheres. The ancillary hfac ligands and the radical backbone are in grey, while the bonds constituting the pathway for the magnetic exchange interaction are highlighted in yellow, with the radical oxygen atoms in red and nitrogen atoms in blue. Some groups of atoms (that is, CF_3, CH_3, and O–CH_3) have been omitted for the sake of clarity. The helices develop along the crystallographic *c* axis of the $P3_1/P3_2$ space groups. The green arrows represent the orientation of the magnetic moments when the magnetic field is applied parallel to the *c* axis, which are not collinear to the field in the case of the anisotropic Co^{II} ions. **c**, Schematic side view of the geometry of the experiment, where needle-like single crystals were mounted on a copper sample holder to form an angle of 15° between the chain direction, **c**, and the propagation vector, **k**, of the X-rays, which is parallel to the applied magnetic field. **d**, Photograph of the sample mounting, viewed from the top, with a ruler as reference.

the 1D Ising model[28]. An activation barrier of about 170 K for the reversal of the magnetization characterizes this material, and magnetic hysteresis in the absence of long-range order is observed below 5 K (ref. 25). Finite-size effects with collective reversal of spin segments[29] and an unprecedented mechanism to control magnetization dynamics through light-induced domain-wall kickoff have also been recently observed in this fascinating material[27].

To investigate the MχD of these 1D molecular crystals, hard X-rays were used to get element-specific information. The excellent stability of the ID12 beamline at ESRF was necessary to investigate single crystals of [Mn-NIT]$_\infty$ and [Co-NIT]$_\infty$ chains with small dimensions ($0.3\times0.3\times8$ mm). X-ray absorption near-edge spectra (XANES) were recorded at the Co and Mn K-edges—that is, transitions promoting electrons from the 1*s* core level—occurring at around 7.7 keV and 6.5 keV, respectively, using the total X-ray fluorescence yield detection mode (see Methods for details).

By recording the XANES spectra with opposite σ^+ (circular left) and σ^- (circular right) polarizations and with a magnetic field applied either parallel (B^+) or antiparallel (B^-) to the X-ray wavevector, we could obtain the three relevant types of dichroism:

$$\mathrm{XNCD} = 1/2\{[\mu(\sigma^-,B^+)-\mu(\sigma^+,B^+)] + [\mu(\sigma^-,B^-)-\mu(\sigma^+,B^-)]\} \quad (1)$$

$$\mathrm{XMCD} = 1/2\{[\mu(\sigma^-,B^+)-\mu(\sigma^+,B^+)] - [\mu(\sigma^-,B^-)-\mu(\sigma^+,B^-)]\} \quad (2)$$

$$\mathrm{XM}\chi\mathrm{D} = \{[\mu(\sigma^-,B^+)+\mu(\sigma^+,B^+)] - [\mu(\sigma^-,B^-)+\mu(\sigma^+,B^-)]\} \quad (3)$$

where $\mu(\sigma,B)$ stands for the absorption measured for the indicated polarization and sign of the magnetic field. XN(M)CD indicate X-ray natural (magnetic) circular dichroism signals and are defined as the difference in absorption spectra recorded with the two circular polarizations. The XNCD signal is independent of the applied magnetic field, whereas XMCD changes its sign when the direction of the applied magnetic field is reversed. The magneto-chiral effect manifests as changes in absorption for two directions of magnetic field, and as such does not require polarized light. To be able to disentangle the XMχD from other dichroic contributions we sum up the spectra recorded with right and left circularly polarized X-rays. The accumulation of the spectra was performed changing field polarity and light helicity in a cyclic way to minimize eventual drift effects in the evaluation of the dichroic quantities. No detectable radiation damage was observed in any of the investigated crystals.

First, room-temperature XNCD spectra were recorded on several crystals to identify two enantiomeric crystals of each [M-NIT]$_\infty$ chain; then the selected crystals were transferred to an experimental station equipped with a 17 T superconducting magnet and constant-flow helium cryostat. These crystals were mounted on the cold finger of the cryostat and oriented with the crystallographic *c* (helix) axis forming an angle of 15° with the vector of propagation of the light **k**, the latter being parallel to the applied magnetic field **B** (Fig. 1c,d). A field of 3 T was employed at $T=5$ K to ensure the magnetic saturation for crystals of both Mn and Co chains and to suppress the slow magnetic relaxation for the latter.

Before describing the results, we briefly recall here some fundamental differences in the interaction between matter and light when moving from ultraviolet–visible to hard X-ray radiation. Because atomic core states are involved in X-ray promoted transitions, the long-wavelength approximation is still valid despite the high energy. Thus the interaction can be expressed in the usual multipolar expansion:

$$H_{\mathrm{int}} = E1+M1+E2 \quad (4)$$

where $E1$ stands for the interaction between the electric dipole and the electric field of the electromagnetic radiation, $M1$ for the interaction between the magnetic dipole and the magnetic field, and $E2$ for the interaction between the electric quadrupole and the electric field gradient. Differently from the ultraviolet–visible region, in X-ray spectroscopy the $M1$ interaction is negligibly small, involving atomic states with different principal quantum number, whereas $E2$ becomes relevant, given its linear dependence with the energy of the transitions.

As the absorption cross section is proportional to the square of the transition matrix element $\left|\langle\varphi_f|H_{\mathrm{int}}|\varphi_i\rangle\right|^2$, with H_{int} from

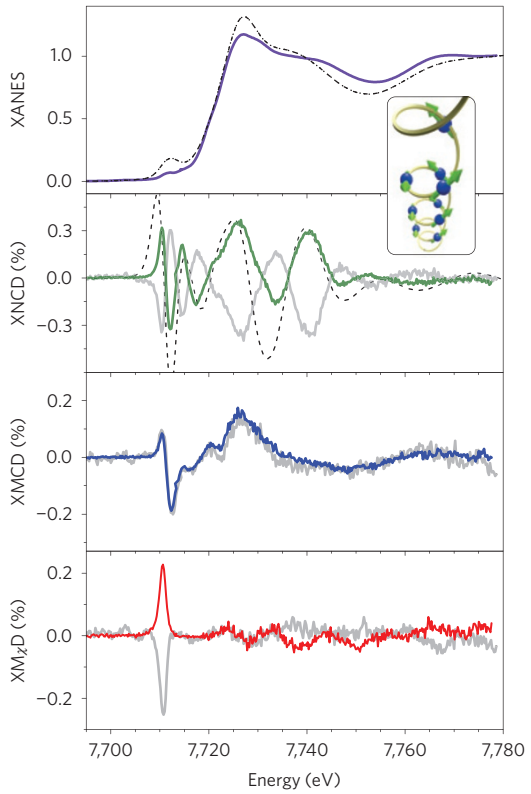

Figure 2 | X-ray absorption and dichroic spectra of the [Co-NIT]$_\infty$ helix. Normalized XANES spectra at the K-edge of Co measured at $B = 3$ T and $T = 5$ K. The dichroic contributions estimated according to equations (1)–(3), and expressed as the percentage of the edge jump in the absorption, are reported for two opposite enantiomers—one in colour and the other in pale grey for clarity. The dashed black lines correspond to the calculated XANES and XNCD for the $P3_1$ enantiomer, whose helicity is visible in the schematic structure drawn in the inset, with arrows representing the non-collinear spin structure of the cobalt helix.

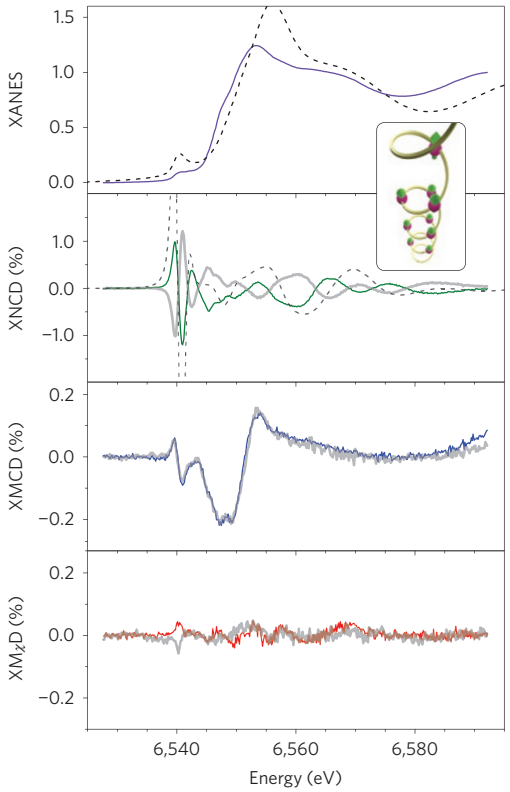

Figure 3 | X-ray absorption and dichroic spectra of the [Mn-NIT]$_\infty$ helix. Normalized XANES spectra at the K-edge of Mn measured at $B = 3$ T and $T = 5$ K. The dichroic contributions estimated according to equations (1)–(3), and expressed as the percentage of the edge jump in the absorption, are reported for two opposite enantiomers—one in colour and other in pale grey for clarity. The dashed black lines correspond to the calculated XANES and XNCD for the $P3_1$ enantiomer, whose helicity is visible in the schematic structure drawn in the inset, with arrows representing the collinear spin structure of the manganese helix.

equation (4), pure electric dipolar ($E1E1$), magnetic dipolar ($M1M1$) and electric quadrupolar ($E2E2$) contributions and two interference terms ($E1M1$) and ($E1E2$) must be considered. The latter is a traceless rank-2 tensor and, in contrast to the pseudoscalar $E1M1$ term, averages to zero in randomly oriented samples. In X-ray spectroscopy it is thus necessary to work with a single crystal or to break artificially the orientational isotropy of space—for example, by dissolving a chiral molecule in an aligned liquid crystal[30].

This drawback, compared to visible–ultraviolet experiments, is fully compensated by the fact that high optical quality and transparency of the crystals is not required. Moreover birefringence is very small, particularly at the high energies employed here. The greatest advantage of X-ray spectroscopy is its element selectivity, which allows discrimination of the magnetic centres.

The different dichroic contributions to X-ray absorption and their symmetry properties are summarized in Table 1. Note that time-reversal symmetry can be broken either by spontaneous magnetic ordering in the sample or by the application of an external magnetic field.

In Fig. 2, the normalized absorption spectrum and corresponding dichroic contributions, obtained according to equations (1)–(3), are shown for two enantiomeric [Co-NIT]$_\infty$ crystals. The dichroic signals are normalized to the corresponding X-ray absorption edge jump. The results of similar experiments for the Mn derivatives are reported in Fig. 3.

Figures 2 and 3 unambiguously show that the three detected dichroic signals, when compared for enantiomeric crystals, are in agreement with the symmetry properties reported in Table 1. Non-zero XNCD and XMχD signals are indeed compatible with the crystal symmetry. In fact, the $P3_1/P3_2$ space groups are among the few types exhibiting all magneto-electric effects, including the existence of toroidal (or anapole) moments[31,32]. As MχD is in general a weak phenomenon, whose intensity is evaluated as the difference of much larger quantities, the comparison of the three dichroic signals is mandatory. Given the fact that every dichroic signal reverses its sign according to parity and time-reversal symmetries of the involved optical transition (Table 1), the presence of artefacts can be safely excluded.

Beyond parity properties, also the spectral features of the dichroic signals provide useful information. Natural circular dichroism is zero for any pure transition and could be observed in the X-ray range only via an interference $E1E2$ term. This contribution is non-zero only if the system has no inversion symmetry. Absence of inversion symmetry allows the atomic orbitals of different parity (for example, p- and d-) to hybridize. In the case of absorption at the K-edge of transition metals, this corresponds to $3d$–$4p$ hybridization, and the XNCD signal is in fact observed at the pre-edge—the feature at the low-energy side of the absorption edge—of both [Co-NIT]$_\infty$ and [Mn-NIT]$_\infty$ helices, at about 7,710 eV and 6,540 eV, respectively. Interestingly XNCD is significantly different from zero on a wide energy range, about 50 eV, for both [M-NIT]$_\infty$ systems. This implies a significant hybridization of extended states formed by empty orbitals (for example, $4p$–$4d$, $4d$–$5p$, and so on) that is compatible with the low symmetry of the metal site induced

by the ligands. Similar wide-energy XNCD features have also been observed in Nd^{III} (ref. 33) and Ni^{II} (ref. 34) compounds, in which the chirality is induced by the structural arrangement of non-chiral moieties, whereas the XMCD signal for a Co^{II} complex with chiral coordination is present only in the pre-edge region where the 3*d* orbitals contribute predominantly[35].

Both XANES and XNCD were reproduced by calculations performed using the FDMNES (Finite Difference Method Near-Edge Structure) package[36]. The electronic structures around Co and Mn atoms were calculated using multiple scattering theory within the muffin-tin approximation, based on a mono-electronic approach. Calculations were performed for clusters built from crystallographic data for the $P3_1$ space group including hydrogen atoms, and views of the asymmetric units generating the chain structure are provided in Supplementary Fig. 1 together with a list of selected bond distances and angles (Supplementary Table 1). Natural circular dichroism was calculated considering *E*1*E*2 transitions only (see Methods for details). The spectral features of both derivatives are reproduced with a reasonable agreement to assign unambiguously the $P3_1$ space group, whose chirality is shown in the inset of Figs 2 and 3, to the crystals having their spectra drawn in colour in the corresponding figure. The XNCD intensity at the pre-edge is about twice as large as for the $[Mn\text{-}NIT]_\infty$ helix, in agreement with the larger number of holes in the 3*d* orbitals and the larger calculated density-of-states (DOS) of the *d*-orbitals at the Fermi level (reported as Supplementary Fig. 2).

Concerning XMCD, for which interference *E*1*E*2 contributions are forbidden by symmetry considerations, the dichroic signal is due to both the dipolar *E*1*E*1 ($1s \rightarrow 4p$) transitions at the rising edge and to the quadrupolar *E*2*E*2 ($1s \rightarrow 3d$) transitions at the pre-edge part of the spectrum, where the partially occupied 3*d* orbitals are involved. Given the fact that the initial 1*s* state has no spin–orbit coupling, the XMCD at the K-edge is probing only the orbital magnetization of the final states. For a d^5 ion (Mn^{II}), K-edge XMCD at the pre-edge is thus expected to be much weaker than for the Co derivative. Comparing Figs 2 and 3, it is clearly evident that XMCD at the pre-edge is significantly reduced in moving from Co to Mn, despite the magnetization being higher in the latter. In contrast, XMCD at the rising edge, which originates from the orbital polarization of the 4*p* states, is fairly similar for the Co and Mn helices, as expected (see also the calculated *p*-type DOS in Supplementary Fig. 2).

Finally, moving on to X-ray MχD, we notice that it originates from the same interference interaction terms as XNCD, although combined with the orbital magnetization of the final states of the absorbing atom. Here a significant difference is observed between the two systems. $[Co\text{-}NIT]_\infty$ helices exhibit a large XMχD signal whose intensity exceeds that of the XMCD signal. To allow a better comparison with data extracted from ultraviolet–visible spectroscopy, the dichroic contributions have been plotted as their correspondent Kuhn asymmetry—that is, $g = \Delta\mu/\mu$, where μ is the absorption. The results shown in the inset of Fig. 4 reveal that the magneto-chiral effect exceeds 3% of the corresponding absorption and is, thus, a remarkable quantity compared to previous reported values.[17–21,37] For instance XMχD of $[Co\text{-}NIT]_\infty$ is two orders of magnitude stronger than that obtained from preliminary measurements at the K-edge on a Cr^{III}–Ni^{II} molecular ferromagnet[34] or that measured in absorption experiments in the ultraviolet–visible range on a ferromagnetically ordered Cr^{III}–Mn^{II} molecular compound[19].

As far as the spectral shape is concerned, the XMχD signal is completely different from the other dichroic contributions, showing a well-defined narrow peak around 7,710 eV—that is, at the pre-edge. This is nicely in agreement with qualitative expectations—a quantitative analysis of this effect being at present beyond available theoretical models. In fact, the intensity of the magneto-chiral

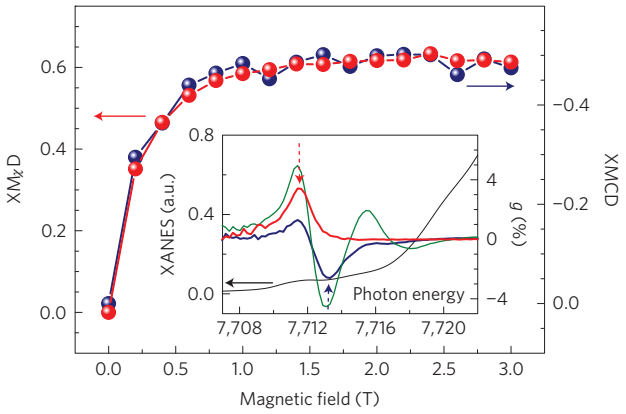

Figure 4 | Field dependence of magnetic and magneto-chiral dichroism of the $[Co\text{-}NIT]_\infty$ helix. XMχD (red spheres) and XMCD (blue spheres) signals in arbitrary units measured at the photon energy of their maximum intensity (see inset) are reported as a function of the magnetic field applied at 15° from the *c* crystallographic axis at $T = 8$ K. In the inset, the photon energy dependence of the intensity of the dichroic contributions (XNCD in green, XMCD in blue, XMχD in red) are reported as the asymmetric ratio $g = \Delta\mu/\mu$; that is, normalizing the signal to the absorption intensity at the same photon energy, which is assumed to be zero before the K-edge. The red and blue arrows indicate the photon energy used to record the field dependence of the corresponding dichroic signals. a.u., arbitrary units.

contribution depends on the interference *E*1*E*2 term, and also on the orbital magnetism of the final state, which is significantly different from zero only where 4*p* orbitals are admixed with partially filled 3*d* orbitals (that is, at the pre-edge), where the calculated DOS (Supplementary Fig. 2) reveals significant contributions from both types of orbitals. A dichroic signal extending on a wider spectral region is instead observed for XNCD due to hybridized extended empty orbitals, such as 4*p*–4*d*, 4*d*–5*p*, and so on.

Moving on to the $[Mn\text{-}NIT]_\infty$ helix, Fig. 3 reveals a marked decrease of the XMχD signal, which becomes hardly detectable. The intensity of magneto-chiral dichroism is often assumed in the literature to be proportional to the product of natural and magnetic dichroism[38], but a rigorous general treatment has not yet been developed. Our element-selective experiments clearly show the limited validity of this assumption in the hard X-ray range.

To get a deeper understanding of this phenomenon, we have also checked how XMCD and XMχD depend on the extent of magnetization of the absorbing atoms by performing the experiment on the $[Co\text{-}NIT]_\infty$ helix as a function of applied magnetic fields in the range 0–3 T at $T = 8$ K; thus, above the freezing temperature of the magnetization of this slow-relaxing material. The field dependence of the maximum signal, measured at 7,713.2 and 7,711.5 eV for XMCD and XMχD, respectively, is reported in Fig. 4. The experiment unambiguously reveals that the two dichroic contributions have exactly the same field dependence, suggesting that the magnetization of the absorbing atoms enters directly in the magneto-chiral effect.

It is interesting to frame our results in the current knowledge of this relatively recent and still unexplored magneto-optical effect. Here all chiral contributions to X-ray absorption spectra are simultaneously detected and their lineshapes are analysed. Moreover, we have found that MχD at the Co K-edge is as large as the other dichroic contributions. A very large XMχD, $g \sim 1\%$ at room temperature, has been recently reported for a chiral paramagnetic molecule comprising terbium(III) and nickel(II) atoms[21]. Surprisingly, the effect was detected only at the L_3-edge of Tb, despite there being no symmetry reasons that should hamper its observation at the L_2-edge. This clearly shows how elusive the detection of the

magneto-chiral effect can be, and underlines the relevance of a complete characterization such as the one presented here.

Additional information can be extracted by the unprecedented possibility of comparing the magneto-chiral behaviour of two isostructural 1D systems showing very different magnetic properties. First, it is clearly evident that the asymmetry factor of the magneto-chiral effect in this energy range is not simply the product of the natural and magnetic effects, because in this approximation a large signal should be observed over a wide energy range and much stronger XMχD should be observed for [Mn-NIT]$_\infty$. Furthermore, the XMχD signal is significant only for transitions involving 3*d* partially filled orbitals and only in the presence of a strong orbital contribution, as in the case of a d^7 ion in an octahedral environment, which is responsible for the non-collinear spin arrangement along the [Co-NIT]$_\infty$ helix.

It would be interesting to investigate if the three-fold screw axis generating the molecular [M-NIT]$_\infty$ helices plays a significant role in the large MχD observed here. Other chains comprising the same building blocks and differing only in the organic group on the radical—aliphatic instead of aromatic (Supplementary Fig. 3)—have been structurally and magnetically characterized, but unfortunately all of them crystallize in centrosymmetric space groups[39]. However, thanks to the element selectivity of the X-ray absorption, it has been possible to compute the XNCD of acentric mixed-metal structures artificially segregating Co and Mn on sites of opposite parity compared to the inversion centre (Supplementary Fig. 4 and Note 1). The results, obtained using the previously described computational approach, reveal a significant decrease, to about 1/3 of the XNCD calculated signal, when moving from the $P3_1/P3_2$ to the $P2_1$ crystal space group, as shown in Supplementary Fig. 5. As the trigonal space group of the investigated helices is induced by the π-stacking interactions between the aromatic substituent on the radical and the hfac ligand on the metal[39], a route to enhance the magneto-chiral effect in molecular materials through a rational chemical design can be envisaged.

In conclusion, the investigated magnetic molecular helices are a model system to study the magneto-chiral effect in detail. The symmetry of the material is compatible with a large variety of magneto-electric effects[22,23,40], still poorly investigated in molecular materials. According to sum rules[41,42], the X-ray MχD could be associated with the presence of an atomic anapole orbital moment, Ω_L, originating from toroidal orbital currents centred on the cobalt atoms. These orbital currents, of relevance for many phenomena ranging from multiferroicity[22,23] to superconductivity[43], originate from the hybridized 3*d*–4*p* states, allowed by the absence of inversion symmetry of the coordination environment around the atom, and therefore they are much stronger that what one would expect for those induced by parity breaking due to the electroweak interaction. It is important to underline that this atomic anapole orbital moment should not be confused with the macroscopic toroidal moment[27] that could originate from the peculiar non-collinear orientation of the magnetic moments along the three-fold helix, which is compatible with Dzyaloshinskii–Moriya interactions. However, to investigate this additional contribution, a less local probe—namely, ultraviolet–visible light—is necessary. Last, but not least, we recall that the [Co-NIT]$_\infty$ molecular helix presents the additional feature of magnetic bistability in the paramagnetic phase. This system thus seems a good candidate for the detection of the 'inverse' magneto-chiral effect—that is, the induction of magnetic polarization in a chiral system by irradiation with non-polarized light. In the scenario of light–matter interaction, this effect, although theoretically predicted[44], is the one still not evidenced by experiments[40]. The possibility to freeze, at low temperature, the light-induced magnetization of this bistable molecular material should facilitate the detection of a weak inverse magneto-chiral effect.

Methods

Crystals of [Mn(hfac)$_2$NITPhOMe]$_\infty$ and [Co(hfac)$_2$NITPhOMe]$_\infty$ were prepared as previously reported[24,39]. Single crystals with needle shape and approximate largest dimensions $10 \times 0.5 \times 0.5\,mm^3$ were selected and checked for the absence of twinning with an Oxford Diffraction single-crystal diffractometer.

The X-ray absorption experiments were carried out at the ID12 beamline of the European Synchrotron Radiation Facility (ESRF), which is dedicated to polarization-dependent X-ray spectroscopy in the photon energy range from 2 to 15 keV (ref. 45). For experiments at the Mn and Co K-edge the source was the helical undulator APPLE-II, which provides a high flux of either right or left circularly polarized X-rays photons with a polarization rate in excess of 0.95. The helicity could be changed in a time less than 5 s. X-rays were monochromatized by the Si⟨111⟩ double-crystal monochromator, ensuring an energy resolution better than the intrinsic broadening due to the finite core-hole lifetime. The samples were mounted on the cold finger of a constant-flow helium cryostat inserted in the bore of a superconducting solenoid producing a magnetic field up to 17 T. The sweep rate to reverse the direction of magnetic field rate was $2\,T\,min^{-1}$. All spectra were recorded in total X-ray fluorescence detection mode in a backscattering geometry using Si photodiodes. The total X-ray fluorescence signal in this energy range is expected to be isotropic. Either the helicity of the incoming X-rays or the direction of magnetic field were changed after each consecutive energy scan to minimize any eventual artefacts in the measurements.

The XANES and XNCD spectra were simulated using the FDMNES code[36]. Calculations were performed for clusters built from crystallographic data for the $P3_1$ space group including hydrogen atoms. Crystallographic data are available from the Cambridge Structural Database (www.ccdc.cam.ac.uk/Community/Requestastructure/Pages/Requestastructure.aspx) using the doi codes http://dx.doi.org/10.1021/ic00020a029 and http://dx.doi.org/10.1039/B004244G for Mn and Co derivatives, respectively. Natural circular dichroism was calculated considering *E*1*E*2 transitions only. Self-consistent calculations including relativistic effects were also performed, and similar results were obtained. Clusters of radius of 14 Å were employed to reproduce the main features in the XNCD, as a further increase of the cluster size did not lead to any improvement. The same procedure was repeated for an aliphatic radical analogue[46] crystallizing in the centrosymmetric $P2_1$/c space group (use doi code http://dx.doi.org/10.1021/ic00283a018 to retrieve crystallographic data from the database mentioned above) by replacing the Mn atoms on the screw axis of opposite chirality, generated by the inversion centre, with Co atoms. The structural similarity between the Mn and Co derivatives and their complete miscibility to form mixed species suggest that no significant structural stress is induced in this artificial model. The spectra were convolved with a Lorentzian with an energy-dependent width, to take into account the core-hole lifetime, and with a Gaussian line, to account for the energy resolution of monochromator. The calculated absorption cross-sections were normalized to the same edge jump to the continuum as in the experiment.

Received 22 June 2014; accepted 9 October 2014; published online 8 December 2014

References

1. Pasteur, L. La dissymétrie moléculaire. Conférence faite le 22 décembre 1883. *Rev. Sci.* **7,** 2–6 (1884).
2. Bordacs, S. *et al.* Chirality of matter shows up via spin excitations. *Nature Phys.* **8,** 734–738 (2012).
3. Mühlbauer, S. *et al.* Skyrmion lattice in a chiral magnet. *Science* **323,** 915–919 (2009).
4. Fert, A., Cros, V. & Sampaio, J. Skyrmions on the track. *Nature Nanotech.* **8,** 152–156 (2013).
5. Romming, N. *et al.* Writing and deleting single magnetic skyrmions. *Science* **341,** 636–639 (2013).
6. Pop, F., Auban-Senzier, P., Canadell, E., Rikken, G. L. J. A. & Avarvari, N. Electrical magnetochiral anisotropy in a bulk chiral molecular conductor. *Nature Commun.* **5,** 3757 (2014).
7. Wagnière, G. & Meier, A. The influence of a static magnetic field on the absorption coefficient of a chiral molecule. *Chem. Phys. Lett.* **93,** 78–81 (1982).
8. Groenewege, M. P. A theory of magneto-optical rotation in diamagnetic molecules of low symmetry. *Mol. Phys.* **5,** 541–563 (1962).
9. Barron, L. D. & Vrbancich, J. Magneto-chiral birefringence and dichroism. *Mol. Phys.* **51,** 715–730 (1984).
10. Baranova, N. B., Bogdanov, Y. V. & Zel'Dovich, B. Y. Electrical analog of the Faraday effect and other new optical effects in liquids. *Opt. Commun.* **22,** 243–247 (1977).
11. Rikken, G. & Raupach, E. Observation of magneto-chiral dichroism. *Nature* **390,** 493–494 (1997).
12. Goulon, J. *et al.* X-ray magnetochiral dichroism: A new spectroscopic probe of parity nonconserving magnetic solids. *Phys. Rev. Lett.* **88,** 237401 (2002).

13. Wagnière, G. H. *On Chiralty and the Universal Asymmetry* (Verlag Helvetica Chimica Acta, 2007).
14. Guijarro, A. & Yus, M. *The Origin of Chirality in the Molecules of Life* (Royal Society of Chemistry, 2009).
15. Rikken, G. L. J. A. & Raupach, E. Enantioselective magnetochiral photochemistry. *Nature* **405,** 932–935 (2000).
16. Zel'dovich, Y. B. Electromagnetic interaction with parity violation. *Sov. Phys. JETP* **6,** 1184–1186 (1958).
17. Vallet, M. *et al.* Observation of magnetochiral birefringence. *Phys. Rev. Lett.* **87,** 183003 (2001).
18. Kubota, M. *et al.* X-ray directional dichroism of a polar ferrimagnet. *Phys. Rev. Lett.* **92,** 137401 (2004).
19. Train, C. *et al.* Strong magneto-chiral dichroism in enantiopure chiral ferromagnets. *Nature Mater.* **7,** 729–734 (2008).
20. Kitagawa, Y., Segawa, H. & Ishii, K. Magneto-chiral dichroism of organic compounds. *Angew. Chem. Int. Ed.* **50,** 9133–9136 (2011).
21. Ceolín, M., Goberna-Ferrón, S. & Galán-Mascarós, J. R. Strong hard X-ray magnetochiral dichroism in paramagnetic enantiopure molecules. *Adv. Mater.* **24,** 3120–3123 (2012).
22. Cheong, S-W. & Mostovoy, M. Multiferroics: A magnetic twist for ferroelectricity. *Nature Mater.* **6,** 13–20 (2007).
23. Khomskii, D. Classifying multiferroics: Mechanisms and effects. *Physics* **2,** 20 (2009).
24. Caneschi, A., Gatteschi, D., Rey, P. & Sessoli, R. Structure and magnetic-ordering of a ferrimagnetic helix formed by manganese(II) and a nitronyl nitroxide radical. *Inorg. Chem.* **30,** 3936–3941 (1991).
25. Caneschi, A. *et al.* Cobalt(II)-nitronyl nitroxide chains as molecular magnetic nanowires. *Angew. Chem. Int. Ed.* **40,** 1760–1763 (2001).
26. Cavigli, L., Sessoli, R., Gurioli, M. & Bogani, L. Second harmonic generation in a molecular magnetic chain. *Phys. Status Solidi A* **203,** 1402–1408 (2006).
27. Heintze, E. *et al.* Dynamic control of magnetic nanowires by light-induced domain-wall kickoffs. *Nature Mater.* **12,** 202–206 (2013).
28. Glauber, R. J. Time-dependent statistic of the Ising model. *J. Math. Phys.* **4,** 294–307 (1963).
29. Bogani, L. *et al.* Finite-size effects in single chain magnets: An experimental and theoretical study. *Phys. Rev. Lett.* **92,** 207204 (2004).
30. Goulon, J. *et al.* X-ray optical activity: Applications of sum rules. *JETP* **97,** 402–431 (2003).
31. Spaldin, N. A., Fiebig, M. & Mostovoy, M. The toroidal moment in condensed-matter physics and its relation to the magnetoelectric effect. *J. Phys. Condens. Matter* **20,** 434203 (2008).
32. Szaller, D., Bordács, S. & Kézsmárki, I. Symmetry conditions for nonreciprocal light propagation in magnetic crystals. *Phys. Rev. B* **87,** 014421 (2013).
33. Alagna, L. *et al.* X-ray natural circular dichroism. *Phys. Rev. Lett.* **80,** 4799–4802 (1998).
34. Goulon, J., Rogalev, A. & Brouder, C. *Comprehensive Chiroptical Spectroscopy* 457–491 (John Wiley, 2012).
35. Stewart, B. *et al.* Circular dichroism at the edge: Large X-ray natural CD in the $1s \rightarrow 3d$ pre-edge feature of $2[Co(en)_3Cl_3]\cdot NaCl\cdot 6H_2O$. *J. Am. Chem. Soc.* **121,** 10233–10234 (1999).
36. Bunău, O. & Joly, Y. Self-consistent aspects of x-ray absorption calculations. *J. Phys. Condens. Matter* **21,** 345501 (2009).
37. Kitagawa, Y., Miyatake, T. & Ishii, K. Magneto-chiral dichroism of artificial light-harvesting antenna. *Chem. Commun.* **48,** 5091–5093 (2012).
38. Rikken, G. & Raupach, E. Pure and cascaded magnetochiral anisotropy in optical absorption. *Phys. Rev. E* **58,** 5081–5084 (1998).
39. Caneschi, A., Gatteschi, D., Lalioti, N., Sangregorio, C. & Sessoli, R. Supramolecular interactions and magnetism of metal-radical chains. *J. Chem. Soc. Dalton Trans.* 3907–3912 (2000).
40. Kibayashi, S., Takahashi, Y., Seki, S. & Tokura, Y. Magnetochiral dichroism resonant with electromagnons in a helimagnet. *Nature Commun.* **5,** 4583 (2014).
41. Carra, P., Jerez, A. & Marri, I. X-ray dichroism in noncentrosymmetric crystals. *Phys. Rev. B* **67,** 045111 (2003).
42. Lovesey, S. W. & Balcar, E. Quantum theory of natural circular, magneto-chiral and non-reciprocal linear dichroism. *Phys. Scr.* **81,** 065703 (2010).
43. Scagnoli, V. *et al.* Observation of orbital currents in CuO. *Science* **332,** 696–698 (2011).
44. Wagnière, G. Inverse magnetochiral birefringence. *Phys. Rev. A* **40,** 2437–2440 (1989).
45. Rogalev, A., Goulon, J., Goulon-Ginet, C. & Malgrange, C. in *Magnetism and Synchrotron Radiation: Lecture Notes in Physics* (eds Beaurepaire, E., Scheurer, F., Krill, G. & Kappler, J. P.) 61 (Springer, 2001).
46. Caneschi, A., Gatteschi, D., Rey, P. & Sessoli, R. Structure and magnetic-properties of ferrimagnetic chains formed by manganese(II) and nitronyl nitroxides. *Inorg. Chem.* **27,** 1756–1761 (1988).

Acknowledgements

We acknowledge the financial contribution of the European Research Council through the AdG MolNanoMaS (267746). The support of ESRF through beamtime allocation (projects HE-3896 and HC-972) is acknowledged. We are indebted to Y. Joly for assistance in spectra simulation and to R. Caciuffo, Ph. Sainctavit and J. Villain for stimulating discussions.

Author contributions

R.S. and A.R. designed the experiment. A.C. synthesized the materials and grew the crystals. M-E.B. carried out preliminary crystallographic and magnetic analysis. M-E.B., M.M., L.P., R.S., F.W. and A.R. participated in the synchrotron experiments and analysed the data. F.W. simulated the XANES and XNCD spectra. R.S. and A.R. wrote the manuscript with contributions from all authors.

Additional information

Supplementary information is available in the online version of the paper. Reprints and permissions information is available online at www.nature.com/reprints. Correspondence and requests for materials should be addressed to R.S.

Competing financial interests

The authors declare no competing financial interests.